LETTER

ACS chemical biology

Designed TPR Modules as Novel Anticancer Agents

Aitziber L. Cortajarena[†], Fang Yi[†], and Lynne Regan[†,‡,*]

[†]Departments of Molecular Biophysics & Biochemistry and [‡]Chemistry, Yale University, 266 Whitney Avenue, New Haven, Connecticut 06520

ABSTRACT Molecules specifically designed to modulate protein–protein interactions have tremendous potential as novel therapeutic agents. One important anticancer target is the chaperone Hsp90, whose activity is essential for the folding of many oncogenic proteins, including HER2, IGFIR, AKT, RAF-1, and FLT-3. Here we report the design and characterization of new tetratricopeptide repeat modules, which bind to the C-terminus of Hsp90 with higher affinity and with greater specificity than natural Hsp90-binding co-chaperones. Thus, when these modules are introduced into the cell, they outcompete endogenous co-chaperones for binding, thereby inhibiting Hsp90 function. The effect of Hsp90 inhibition in this fashion is dramatic; HER2 levels are substantially decreased and BT474 HER2 positive breast cancer cells are killed. Our designs thus provide new tools with which to dissect the mechanism of Hsp90-mediated protein folding and also open the door to the development of an entirely new class of anticancer agents.

Inhibition of protein–protein interactions to control cellular processes and as a route to novel therapeutics is an exciting yet undeveloped vision. In this Letter we realize this concept in the context of the protein chaperone Hsp90. Because many oncogenic proteins are clients of Hsp90, inhibitors of Hsp90 are sought as potential anticancer agents. For example, over one-quarter of all breast cancers are HER2 positive, that is, they overexpress the cell-surface protein HER2, and the aggressiveness of cancer growth is proportional to the amount of HER2 produced (*1, 2*). Hsp90 is essential for the correct folding and maturation of HER2 and is involved in many interactions with other proteins. Indeed, the functional form of Hsp90 is a complex in which the chaperones Hsp90 and Hsp70 are brought together by binding to Hsp Organizing Protein (HOP) (*3*). Assembly of this multiprotein complex is achieved by means of two independent tetratricopeptide repeat (TPR) domains on HOP: TPR1, which binds to the C-terminal tail of Hsp70, and TPR2A, which binds to the C-terminal tail of Hsp90 (Figure 1) (*4*). Hsp90 activity is essential for the folding of many oncogenic proteins beyond HER2, including IGFIR, AKT, RAF-1, and FLT-3, each of which is associated with a different type of cancer (*5–8*). Inhibition of the interaction of Hsp90 with HOP, that is, inhibition of the TPR2A–Hsp90 interaction, thus represents a new and generally applicable approach to the development of anticancer agents.

TPR1 and TPR2A bind their cognate ligands with dissociation constants of about 50 and 5 μM, respectively. The C-terminal peptides of Hsp70 and Hsp90 are similar in sequence (see Figure 3, panel b), nevertheless both TPR1 and TPR2A discriminate against their noncognate ligands. We have designed a TPR module, CTPR3, which is significantly more stable than either TPR1 or TPR2A and thus represents a robust scaffold on which to introduce novel activities (the melting temperature of CTPR3 is 83 °C, compared to about 50 °C for both TPR1 and TPR2A) (*9*). We grafted the Hsp90-binding residues from TPR2A onto the CTPR3 scaffold to create a module that we named CTPR390 (*10*). We showed that CTPR390 binds preferentially to the C-terminal peptide of Hsp90, with moderate affinity (Figure 3, panel a). To better understand the details of the interaction of CTPR390 with the Hsp90 peptide and to guide designs for higher affinity binding, we determined the crystal structure of CTPR390 in complex with the C-terminal peptide of Hsp90 (Figure 2, panel a; Table 1). The peptide is clearly visible, bound in the concave groove of the TPR, in contact with the grafted Hsp90-binding residues. The interactions between the peptide and CTPR390 are similar to those observed in the structure of the TPR2A–Hsp90 complex (*11*). For example, Lys13, Asn17, Asn48, Asn51, and Arg82 make hydrogen bonds to the peptide backbone, and Tyr20, Lys21, Lys78, and Arg82 interact with peptide side chains. However,

***Corresponding author,**
lynne.regan@yale.edu.

Received for review December 18, 2007 and accepted January 16, 2008.

Published online March 20, 2008

10.1021/cb700260z CCC: $40.75

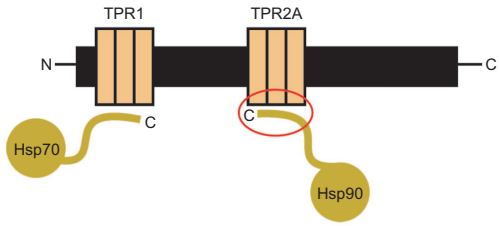

Figure 1. Hsp Organizing Protein (HOP). Schematic representation of HOP protein indicating the two independent TPR domains, TPR1 and TPR2A, which interact with the C-terminal tails of Hsp70 and Hsp90, respectively. The circle highlights the TPR2A-Hsp90 interaction.

not all of the TPR−peptide interactions seen in the TPR2A−Hsp90 complex are present or optimized in the CTPR390− peptide complex, consistent with the observation that CTPR390 binds to the Hsp90 peptide more weakly than does TPR2A.

In a second round of designs, we sought to improve the affinity of the designed TPR for the Hsp90 peptide. Because electrostatic interactions play a key role in TPR−peptide binding, we investigated the possibility of modulating binding affinity by re-engineering the charge on the back face of the TPR. The CTPR390−, CTPR390, and CTPR390+ designs all have the peptide recognition residues from TPR2A grafted onto the CTPR3 framework but have negative, neutral, or positively charged back faces, respectively (Figure 2, panel b). It is possible to engineer such dramatic changes in charge because the designed CTPR3 module is robust and can accommodate many modifications.

We measured the binding affinity of the three charge variants, CTPR390−, CTPR390, and CTRP390+, to the C-terminal peptide of Hsp90. It is clear from the data presented in Figure 3, panel a, that the charge on the back face has a significant effect on the affinity of the TPR protein for the peptide. Binding affinity increases dramatically as the charge on the back face becomes more positive, with a dissociation constant for the CTPR390+ Hsp90 peptide interaction of less than 1 μM. Thus CTPR390+ binds to the C-terminal peptide of Hsp90 more tightly than the TPR2A domain of HOP. Not only affinity but also specificity is critical for functional ligand binding *in vivo*. We therefore tested the binding of CTPR390+ to the C-terminal peptides of both Hsp90 and Hsp70. The data in Figure 3, panel b clearly show that CTPR390+ discriminates against the noncognate Hsp70 ligand extremely well. Under the typical assay conditions, binding to Hsp70 peptide is essentially undetectable. We therefore estimate that CTPR390+ binds to Hsp90 at least 100−1000 times more tightly than it binds to Hsp70. This discrimination between cognate and noncognate ligands is much greater than that of TPR2A, which prefers cognate over noncognate ligand by only about 10-fold.

Hsp90 functions in multichaperone complexes to aid in the folding and maturation of its client proteins (*12, 13*). Previous studies have shown that overexpression of the TPR domain of protein phosphatase 5 in CV-1 cells causes a decrease in Hsp90-mediated glucocorticoid receptor maturation (*14, 15*). CTPR390+ binds tightly and specifically to Hsp90 and therefore has the potential to compete with endogenous TPR containing co-chaperones for binding to Hsp90. Inhibiting the formation of the correct Hsp90−co-chaperone complexes *in vivo* should inhibit Hsp90 activity and thus prevent the folding of Hsp90-dependent client proteins. We therefore tested the effect of CTPR390+ *in vivo* using BT474 HER2 positive breast ductal carcinoma cells. Purified CTPR390+ was introduced into BT474 cells using ProteoJuice (Novagen). We confirmed that CTPR modules could be deliv-

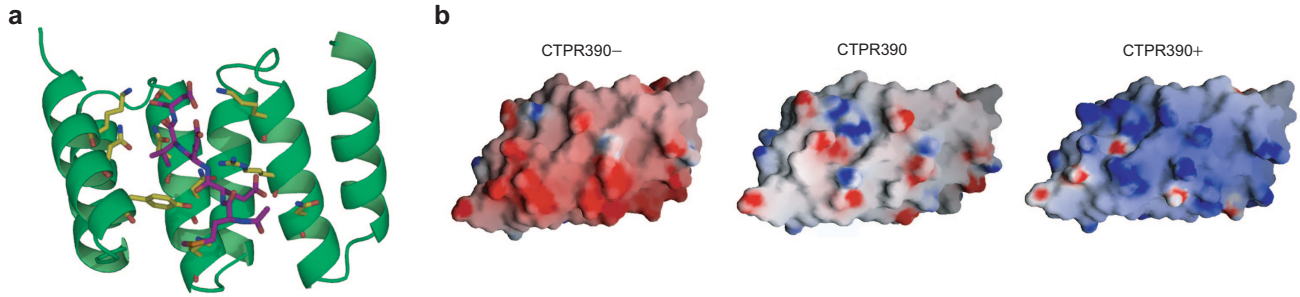

Figure 2. CTPR390 designed proteins. a) X-ray crystal structure of CTPR390 in complex with the C-terminal peptide of Hsp90. The backbone of CTPR390 is shown as a ribbon, and side chains of residues of the TPR that directly interact with the peptide are displayed as sticks in yellow. The C-terminal Hsp90 peptide is shown as sticks in purple. b) Surface representation of the electrostatic potential of the back/convex face of CTPR390− (negative back face), CTPR390 (neutral back face), and CTPR390+ (positive back face). The color range, from deep red to deep blue, corresponds to values of the electrostatic potential from −16 to + 20 $kT\,e^{-1}$, where *k* is the Boltzmann constant, *T* is absolute temperature, and e is a proton's charge. The figures were produced using GRASP (http://trantor.bioc.columbia.edu/grasp/) (*32*).

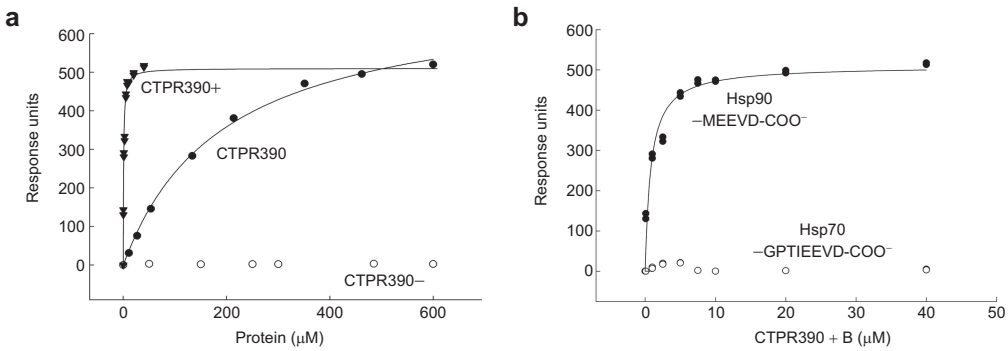

Figure 3. Binding activity and specificity of the CTPR390 proteins. a) Plot of equilibrium response levels (response units) versus protein concentration for CTPR390− (negative), CTPR390 (neutral), and CTPR390+ (positive). All proteins were tested for binding to an N-terminally biotinylated peptide, which corresponds to the C-terminal peptide of Hsp90, attached to a neutravidin chip. TPR binding is monitored by surface plasmon resonance (SPR). The dissociation constants were calculated by fitting the data to a steady state 1:1 binding model and are $K_{D\ CTPR390/Hsp90}$ = 200 μM; $K_{D\ CTPR390+/Hsp90}$ = 1 μM; $K_{D\ CTPR390-/Hsp90}$ too weak to measure). b) Comparison of the binding of CTPR390+ to the Hsp90 and Hsp70. N-terminally biotinylated peptides corresponding to the C-termini of Hsp70 or Hsp90 were attached to neutravidin chips, and binding of CTPR390+ was monitored by SPR. The corresponding C-terminal sequences of the Hsp70 and Hsp90 peptides are shown. Equilibrium response levels (response units) are plotted versus protein concentration.

ered in this fashion, by using fluorescence microscopy to detect the intracellular delivery of Alexa-labeled CTPR390+. To test the effects of CTPR390+ treatment on the levels of Hsp90 client proteins, we used Western blot analysis to compare the amounts of HER2 and phosphorylated HER2 (the functional form of HER2) relative to the amount of a non-Hsp90-dependent control protein, glyceraldehyde-3-phosphate dehydrogenase (GAPDH) (Figure 4; also see Supplemental Note in Supporting Information). Clear concentration- and time-dependent decreases in the levels of HER2 and phosphorylated HER2 were observed when the cells were treated with CTPR390+. The reductions in HER2 and phosphorylated HER2 levels are significant, with the levels of phosphorylated HER2 decreasing to less than 20% of the starting value at the longest post-treatment time-point.

It has been shown that inhibition of Hsp90 by the N-terminal active site inhibitor 17-AAG results in a significant decrease in the cellular levels of Hsp90-dependent proteins, for example, HER2 in breast cancer cells. 17-AAG is now in clinical trials as a treatment for several different cancer types (*16, 17*). A side effect of the inhibition of Hsp90 with 17-AAG-like inhibitors is the induction of Hsp70 production. Induction of Hsp70 is undesirable, because its antiapoptotic function counteracts the effect of Hsp90 inhibition (*18, 19*). We therefore tested the effect of CTPR390+ treatment on Hsp70 levels in BT474 cells. Figure 4 shows Western blot analysis of BT474 extracts after treatment of the cells with CTPR390+. No induction of Hsp70 is observed.

In summary, we have designed a TPR module, CTPR390+, which is more stable and binds more tightly and more specifically to Hsp90 than endogenous Hsp90-binding co-chaperones. Treatment of BT474 cells with CTPR390+ results in a decrease in the levels of HER2 with consequent inhibition of cell proliferation. Furthermore, inhibition of Hsp90 in this fashion does not result in the undesired elevation of Hsp70 levels. To our knowledge, this is the first example of using

TABLE 1. Data collection and refinement statistics

	CTPR390−Hsp90
Space group	*R*3
Unit cell dimensions	
a, *b*, *c* (Å)	100.67, 100.67, 161.57
α, β, γ (deg)	90, 90, 120
Resolution (Å)	30–2.85
R_{merge} (%)[a]	7.5 (39.7)
$I/\sigma I$[a]	21.18 (1.16)
Completeness (%)[a]	99.4 (99.7)
Redundancy[a]	5.18 (5.28)
Unique reflections	13878
R_{work}/R_{free}	27.1/28.2
RMSD bond (Å)	0.005
RMSD angle (deg)	0.708

[a]Values in parentheses correspond to the highest resolution bin.

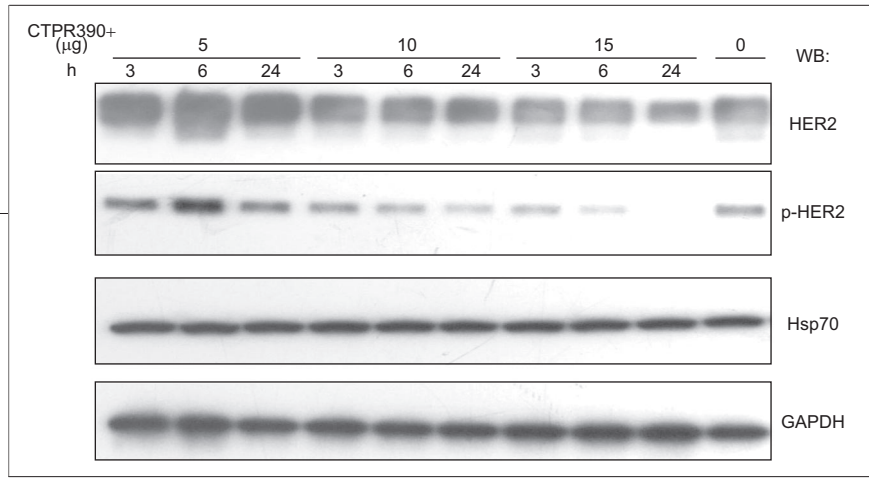

Figure 4. CTPR390+ down regulates HER2 and phosphorylated HER2 levels *in vivo*. CTPR390+ protein (5, 10, and 15 μg) was transfected into BT474 cells, and the cells were harvested 3, 6, and 24 h post-transfection. Cell lysates (25 μg total protein for each sample) were analyzed by Western blotting, probing with antibodies specific for HER2, phosphorylated-HER2, Hsp70, and GAPDH. ProteoJuice alone did not show any effects on HER2 expression levels.

an engineered Hsp90-binding TPR to inhibit chaperone function. Our designs thus provide new tools with which to dissect the mechanism of Hsp90-mediated protein folding. Moreover, although here we achieve inhibition *in vivo* using a designed protein, for therapeutic applications one can easily imagine inhibiting Hsp90 in this same novel fashion, but using a small molecule.

METHODS

Protein Design. CTPR3, which is the framework for the functional designs, was created and characterized as previously described (*9*). One TPR repeat contains two tandem α-helices, which we refer to as the A and B helices. CTPR390−,CTPR390, and CTPR390+ all incorporate the same ligand-binding residues (*10*), such that the sequences of the first, second, and third A helices of all of these proteins are as follows: first A helix = AEAWKNLGNAYYK; second A helix = ASAWYNLGNAYYK; third A helix = AKAWYRRGNAYYK. CTPR390−, CTPR390, and CTPR390+ differ in their back face charge. This was accomplished by manipulating the sequence of the solvent-exposed B helix, at positions that statistical analyses of all TPR sequences show can accommodate either negatively or positively charged residues (*20*). Within each of these proteins, the sequence of the first, second, and third B helices are the same. The repeated B-helix sequence in CTPR390− is DYDEAIEYYQKALEL, in CTPR390 it is DYQKAIEYYQKALEL, and in CTPR390+ it is KYQKAIKYYQKALKL. Underlined residues highlight the positions of the solvent-exposed charged residues.

Cloning and Molecular Biology. Genes encoding the TPR proteins were constructed as previously described (*10, 21*). The final product was subcloned into the pProEx-HTA vector (GibcoBRL, Gaithersburg, MD) to create genes incorporating an N-terminal His6-tag, followed by a TEV cleavage site. Construct identity was verified by DNA sequencing (W. M. Keck Facility, Yale University, New Haven).

Protein Expression and Purification. All proteins were overexpressed and purified, essentially as previously described (*9, 10, 21*). As a final step, protein was loaded onto a size exclusion column, the HiLoad Superdex HR-75 column (Amersham Bioscience, Uppsala, Sweden). Protein concentration was measured by UV absorbance at 280 nm, using extinction coefficients at 280 nm calculated from amino acid composition (*22*).

Protein Crystallization and Data Collection. Purified CTPR390 protein was concentrated to 20 mg mL^{-1} in 10 mM Tris-HCl, 50 mM NaCl, pH 7.5. Crystals of CTPR390 in complex with the C-terminal five amino acids of Hsp90 (Ac-MEEVD-COOH peptide) using a protein to peptide ratio of 1:4 were obtained at 295 K. Using microbatch-under-oil screening at the high-throughput crystallization laboratory at the Hauptman-Woodward Medical Research Institute Inc. (HWI, Buffalo, NY) (*23*), a few crystallization conditions were identified. Only one crystallization condition (0.1 M NaH_2PO_4, 40% (w/v) PEG 20 000, 0.1 M CAPS, pH 10.0) could be reproduced in our laboratory, and we optimized that condition by the sitting-drop vapor diffusion method, using 2-fold diluted initial formulation as the well solution. The final crystallization condition contained 50 mM NaH_2PO_4, 20% (w/v) PEG 20 000, and 50 mM CAPS, pH 10.0. The well solution was mixed in equal volumes (2 μL) with a protein−peptide complex solution (1:4 molar ratio) at 30 mg mL^{-1} protein concentration. Crystals appeared within 1 week and reached sizes of approximately 80 × 80 × 50 $μm^3$ within 2 weeks. Crystals were flash-cooled under a nitrogen gas stream (100 K). Data were collected to 2.85 Å resolution at NSLS beam line X12C, Brookhaven National Laboratory.

Structure Determination and Refinement. The data set was indexed, scaled, and integrated using the HKL2000 program (*24*). The crystal belongs to the space group *R*3 with unit cell dimensions of $a = b = 100.67$ Å, $c = 161.57$ Å and $\alpha = \beta = 90°$, $\gamma = 120°$. The CTPR390 structure was solved by molecular replacement using the program MOLREP (*25*) in the CCP4i suite (*26*). The structure of the consensus TPR, CTPR3 (*9*), was used as search model (PDB id 1NA0), and there were 5 molecules present in the asymmetric unit. The structure was refined with the programs CNS (*27*) and Refmac5 (*28*) with TLS refinement (*29*) in the late stages of the refinement to a resolution of 2.85 Å. Iterative rounds of refinement model adjusting in COOT (*30*) were carried out until *R* factors converged to a final value of $R/R_{free} = 28.4/29.2$ for the structure without ligand–peptide built. The ligand–peptide was built in the difference electron density map $F_o - F_c$ first in the CTPR390 unit with stronger positive density using as starting backbone conformation the Hsp90 peptide from the TPR2A−Hsp90 complex (PDB id 1ELR) (*11*). After refinement of the model with one peptide copy, the other peptides were built by symmetry operations of the refined peptide chain in the binding pockets of the other protein chains, and the complete model was refined. Water molecules were automatically added in COOT and were validated with the electron density maps. The final model with one peptide molecule in each binding groove of the five TPR molecules in the asymmetric unit converged to $R/R_{free} = 27.1/28.2$. The geometry and stereochemical properties of the model was checked with the program Molprobity (*31*). Crystallographic statistics are shown in Table 1. More detailed description of the structure determination will be presented elsewhere; the atomic coordinates are being deposited in the Protein Data Bank.

Surface Plasmon Resonance-Based Binding Assays. Surface plasmon resonance measurements were performed using a BIACORE 3000 (BIACORE AB, Uppsala, Sweden) as previously described (*10*). Neutravidin was immobilized on a CM5 sensor chip through standard amide coupling, and then 200−300 relative units (RU) of N-terminally biotinylated 24-mer peptides of Hsp90 and Hsp70 (W. M. Keck Facility, Yale University, New Haven) were loaded onto the neutravidin chip in HBS-EP buffer (150 mM NaCl, 3 mM EDTA, 0.005% (v/v) polysorbate 20, 10 mM HEPES, pH 7.5). Binding was monitored in RU when TPR proteins were passed over immobilized peptides at different protein concentrations, in HBS-EP buffer, at a flow rate of 40 μL min^{-1} using KINJECT mode. Any nonspecific binding was corrected for by subtraction of binding to neutravidin alone for each TPR concentration tested. The response values (R_{eq}) at the equilibrium were plotted versus the protein concentration, dissociation constants (K_D) were determined by fitting the data to a one-site binding model using the following equation:

$$R_{eq} = \frac{R_{max}[P]}{K_D + [P]}$$

where R_{eq} is the equilibrium response, K_D is the dissociation constant, [P] is the protein concentration in the mobile phase, and R_{max} is the equilibrium response at saturation.

Protein Transfection into BT474 Cells. BT474 is a human ductal breast cancer cell line that endogenously overexpresses HER2. Cells were cultured in RPMI-1640 media supplemented with 10% heat-inactivated fetal bovine serum, 2 mM glutamine, 10 μg mL^{-1} insulin, penicillin, and streptomycin in a humidified atmosphere of 5% CO_2 at 37 °C. Purified CTPR390+ protein was transfected into cultured BT474 cells using ProteoJuice reagent (Novagen) following the procedures recommended by the manufacturer. Briefly, 2×10^5 cells were plated in each well of a 6-well plate 24 h prior to transfection. Transfection mixtures con-

acs chemical biology

sisted of ProteoJuice reagent and different amounts of purified CTPR390+ (5, 10, and 15 μg) and Opti-MEM media in a total volume of 100 μL. The protein and ProteoJuice reagent ratio was 1:1 (v/w). After incubating the transfection mixture at RT for 20 min, another 900 μL of Opti-MEM media was added and mixed. The transfection mixture was added directly to cells in different wells, and they were allowed to grow for 3, 6, and 24 h. Alexa-labeled CTPR390+ protein was transfected under the same conditions to confirm the delivery under the fluorescence microscope. After 3 h of incubation with the cells, the transfection mixture was supplemented with complete media and allowed to grow to 24 h. Prior to performing microscopic or immunoblotting analysis, cells were washed with cold PBS three times to remove any untransfected protein in the media. Cells were photographed on a Nikon Eclipse TE2000-U fluorescence microscope with an X20 objective with X1.5 intermediate magnification.

Western Blot Analysis. For Western blotting, the washed cells were scraped into cold lysis buffer (50 mM Tris-HCl, pH 7.4, 150 mM NaCl, 1 mM EDTA, 1 mM EGTA, 0.1% SDS, 1% NP-40, 1 mM Na_3VO_4, 25 mM NaF, 25 mM β-glycerol-phosphate) supplemented with Complete protease inhibitors (Roche Molecular Biochemicals). After being incubated on ice for 30 min, the lysates were centrifuged at 14,000 rpm (4 °C) for 15 min to remove insoluble material. Total protein concentration was determined using the BCA assay (Pierce). Cell lysates of 25 μg total protein were separated on a 4−12% gradient SDS-polyacrylamide gel (Biorad) followed by transfer to a 0.45 μm PVDF membrane. Membrane was blocked in 5% nonfat milk in Tris-buffered saline containing 0.1% Tween 20 (TBST) with 1 mM Na_3VO_4 for 1 h at RT on a shaker. Primary antibodies were diluted in TBST 5% BSA at concentrations of 1:2000 (anti-HER2,sc-284, Santa Cruz Biotechnology), 1:200 (antiphosphor-HER2, clone PN2A, Neomarkers), and 1:5000 (HRP conjugated anti-GAPDH, ab9482, abCam). Membranes were incubated with the primary antibodies at 4 °C overnight and then washed five times with TBST, at RT. Secondary HRP conjugated antibodies (antimouse antibody from Santa Cruz Biotechnology, Inc., antirabbit from Amersham, antirat from Stressgen/Assay designs) were diluted 1:2000. Membranes were incubated in the secondary antibodies at RT for 1 h and washed 4 times in TBST and once in TBS, followed by chemiluminescent detection (ECL solution, Amersham). Quantitative analysis of the intensity of Western blot bands was performed using Kodak 1D software.

Acknowledgment: We thank Jimin Wang for his x-ray crystallographic advice and also members of staff at NSLS beamlines X12C and X6A, BNL, where data were collected. The high-throughput crystal screening service of the Hauptman-Woodward facility assisted in identifying initial crystallization conditions. BT474 cells were a kind gift from Dr. Michael DiGiovanna. We thank Dr. Sandra Wolin for allowing us to use her cell culture facilities, without which this work would not have been possible. We thank Laura Edwards, Tijana Grove, Meredith Jackrel, Lenka Kundrat, and Simon Mochrie for valuable discussions and comments on the manuscript. F.Y. is a recipient of the Concept Award from the Department of Defense, Breast Cancer Research Program (W91ZSQ7167N696).

Supporting Information Available: This material is free of charge *via* the Internet.

REFERENCES

1. Slamon, D. J., Clark, G. M., Wong, S. G., Levin, W. J., Ullrich, A., and McGuire, W. L. (1987) Human breast cancer: correlation of relapse and survival with amplification of the HER2/neu oncogene, *Science 235*, 177–182.
2. DiGiovanna, M. P. (1999) *Clinical Significance of HER-2/neu Overexpression* Part II., Vol. 13, Lippincott Williams & Wilkins, Cedar Knolls, NJ.
3. Johnson, B. D., Schumacher, R. J., Ross, E. D., and Toft, D. O. (1998) Hop modulates Hsp70/Hsp90 interactions in protein folding, *J. Biol. Chem. 273*, 3679–3686.
4. Brinker, A., Scheufler, C., Von Der Mulbe, F., Fleckenstein, B., Herrmann, C., Jung, G., Moarefi, I., and Hartl, F. U. (2002) Ligand discrimination by TPR domains. Relevance and selectivity of EEVD-recognition in Hsp70x Hop × Hsp90 complexes, *J. Biol. Chem. 277*, 19265–19275.
5. Scott, M. D., and Frydman, J. (2003) Aberrant protein folding as the molecular basis of cancer, *Methods Mol. Biol. 232*, 67–76.
6. Schnur, R. C., Corman, M. L., Gallaschun, R. J., Cooper, B. A., Dee, M. F., Doty, J. l., Muzzi, M. L., DiOrio, C. I., Barbacci, E. G., and Miller, P. E. (1995) erbB-2 oncogene inhibition by geldanamycin derivatives: mechanism of action and structure-activity relationships, *J. Med. Chem. 15*, 3813–3820.
7. Neckers, L., Mimnaugh, E., and Schulte, T. W. (1999) Hsp90 as an anti-cancer target, *Drug Resist. Updates 2*, 165–172.
8. Workman, P., Burrows, F., Neckers, L., and Rosend, N. (2007) Drugging the cancer chaperone Hsp90: Combinatorial therapeutic exploitation of oncogene addiction and tumor stress, *Ann. N.Y. Acad. Sci.* 202–216.
9. Main, E. R. G., Xiong, Y., Cocco, M. J., D'Andrea, L., and Regan, L. (2003) Design of stable α-helical arrays from an idealized TPR motif, *Structure 11*, 497–508.
10. Cortajarena, A. L., Kajander, T., Pan, W., Cocco, M. J., and Regan, L. (2004) Protein design to understand peptide ligand recognition by tetratricopeptide repeat proteins, *Protein Eng., Des. Sel. 17*, 399–409.
11. Scheufler, C., Brinker, A., Bourenkov, G., Pegoraro, S., Moroder, L., Bartunik, H., Hartl, F. U., and Moarefi, I. (2000) Structure of TPR domain-peptide complexes: critical elements in the assembly of the Hsp70-Hsp90 multichaperone machine, *Cell 101*, 199–210.
12. Pearl, L. H., and Prodromou, C. (2006) Structure and mechanism of the Hsp90 molecular chaperone machinery, *Annu. Rev. Biochem. 75*, 271–294.
13. Riggs, D. L., Cox, M. B., Cheung-Flynn, J., Prapapanich, V., Carrigan, P. E., and and Smith, D. F. (2004) Functional specificity of co-chaperone interactions with Hsp90 client proteins, *Crit. Rev. Biochem. Mol. Biol. 39*.
14. Chen, M.-S., Silverstein, A. M., Pratt, W. B., and Chinkers, M. (1996) The tetratricopeptide repeat domain of protein phosphatase 5 mediates binding to glucocorticoid receptor heterocomplexes and acts as a dominant negative mutant, *J. Biol. Chem. 271*, 32315–32320.
15. Brychzy, A., Rein, T., Winklhofer, K. F., Hartl, F. U., Young, J. C., and Obermann, W. M. (2003) Cofactor Tpr2 combines two TPR domains and a J domain to regulate the Hsp70/Hsp90 chaperone system, *EMBO J. 22*, 3613–3623.
16. Nowakowski, G. S., McCollum, A. K., Ames, M. M., Mandrekar, S. J., Reid, J. M., Adjei, A. A., Toft, D. O., Safgren, S. L., and Erlichman, C. (2006) A Phase I trial of twice-weekly 17-allylamino-demethoxy-geldanamycin in patients with advanced cancer, *Clin. Cancer Res. 12*, 6087–6093.
17. Bagatell, R., Beliakoff, J., David, C. L., Marron, M. T., and Whitesell, L. (2005) Hsp90 inhibitors deplete key anti-apoptotic proteins in pediatric solid tumor cells and demonstrate synergistic anticancer activity with cisplatin, *Int. J. Cancer 113*, 179–188.
18. Calderwood, S. K., Khaleque, M. A., Sawyer, D. B., and Ciocca, D. R. (2006) Heat shock proteins in cancer: chaperones of tumorigenesis, *Trends Biochem. Sci. 31*, 164–172.
19. Mosser, D. D., and Morimoto, R. I. (2004) Molecular chaperones and the stress of oncogenesis, *Oncogene 23*, 2907–2918.
20. Magliery, T. J., and Regan, L. (2004) Beyond consensus: statistical free energies reveal hidden interactions in the design of a TPR motif, *J. Mol. Biol. 343*, 731–745.
21. Kajander, T., Cortajarena, A. L., and Regan, L. (2006) Consensus design as a tool for engineering repeat proteins, *Methods Mol. Biol. 340*, 151–170.
22. Pace, C. N., Vajdos, F., Fee, L., Grimsley, G., and Gray, T. (1995) How to measure and predict the molar absorption coefficient of a protein, *Protein Sci. 4*, 2411–2423.
23. Luft, J. R., Collins, R. J., Fehrman, N. A., Lauricella, A. M., Veatch, C. K., and DeTitta, G. T. (2003) A deliberate approach to screening for initial crystallization conditions of biological macromolecules, *J. Struct. Biol. 142*, 170–179.
24. Otwinowski, Z., and Minor, W. (1997) In *Methods in Enzymology* (Carter, C. W. J. , and Sweet, R. M., Eds.) Vol. 276, pp 307–326, Academic Press, New York.
25. Vagin, A. A., and Teplyakov, A. (1997) MOLREP: an automated program for molecular replacement, *J. Appl. Crystallogr. 30*, 1022–1025.
26. Project, C. C. C. (1994) The CCP4 suite: programs for protein crystallography, *Acta Crystallogr., Sect. D 50*, 760–763.
27. Brünger, A. T., Adams, P. D., Clore, G. M., DeLano, W. L., Gros, P., Grosse-Kunstleve, R. W., Jiang, J. S., Kuszewski, J., Nilges, M., Pannu, N. S., Read, R. J., Rice, L. M., Simonson, T., and Warren, G. L. (1998) Crystallography & NMR system: A new software suite for macromolecular structure determination, *Acta Crystallogr., Sect. D 54*, 905–921.

28. Murshudov, G., Vagin, A., and Dodson, E. (1997) Refinement of macromolecular structures by the maximum-likelihood method, *Acta Crystallogr. Sect. D 53*, 240–255.
29. Winn, M., Isupov, M., and Murshudov, G. N. (2001) Use of TLS parameters to model anisotropic displacements in macromolecular refinement, *Acta Crystallogr. Sect. D 57*, 122–133.
30. Emsley, P., and Cowtan, K. (2004) Coot: model-building tools for molecular graphics, *Acta Crystallogr. Sect. D 60*, 2126–2132.
31. Lovell, S. C., Davis, I. W., Arendall, W. B. I., de Bakker, P. I. W., Word, J. M., Prisant, M. G., Richardson, J. S., and Richardson, D. C. (2003) Structure validation by C-alpha geometry: phi, psi, and C-beta deviation, *Proteins: Struct., Funct., Genet. 50*, 437–450.
32. Nicholls, A., Bharadwaj, R., and Honig, B. (1993) GRASP-graphical representation and analysis of surface properties, *Biophys. J. 64*, A166.